Anisotropic Enhancement of Second Harmonic Generation in Monolayer and Bilayer MoS2 by Integrating with TiO2 Nanowires

Article · May 2019

CITATIONS
9

READS
576

12 authors, including:

Dawei Li
Dalian University of Technology
67 PUBLICATIONS **1,068** CITATIONS
SEE PROFILE

Jingfeng Song
University of Connecticut
42 PUBLICATIONS **924** CITATIONS
SEE PROFILE

Xi Huang
University of Nebraska at Lincoln
62 PUBLICATIONS **1,122** CITATIONS
SEE PROFILE

Fei Wang
University of Nebraska at Lincoln
42 PUBLICATIONS **514** CITATIONS
SEE PROFILE

Communication

Anisotropic Enhancement of Second Harmonic Generation in Monolayer and Bilayer MoS by Integrating with TiO Nanowires

Dawei Li, Chengyiran Wei, Jingfeng Song, Xi Huang, fei wang, Kun Liu, Wei Xiong, Xia Hong, Bai Cui, Aixin Feng, Lan Jiang, and Yong Feng Lu

Nano Lett., **Just Accepted Manuscript** • DOI: 10.1021/acs.nanolett.9b01933 • Publication Date (Web): 28 May 2019

Anisotropic Enhancement of Second Harmonic Generation in Monolayer and Bilayer MoS_2 by Integrating with TiO_2 Nanowires

Dawei Li,[†,‖,±,*] *Chengyiran Wei,*[‡,§,±] *Jingfeng Song,*[†] *Xi Huang,*[‡] *Fei Wang,*[Δ] *Kun Liu,*[#] *Wei Xiong,*[§,*] *Xia Hong,*[†] *Bai Cui,*[Δ] *Aixin Feng,*[‖] *Lan Jiang,*[≠] *and Yongfeng Lu* [‡,*]

[†]Department of Physics and Astronomy and Nebraska Center for Materials and Nanoscience, University of Nebraska-Lincoln, Lincoln, NE 68588-0299, United States

[‖]College of Mechanical & Electrical Engineering, Wenzhou University, Wenzhou 325035, China

[‡]Department of Electrical and Computer Engineering, University of Nebraska-Lincoln, Lincoln, NE 68588-0511, United States

[§]Wuhan National Laboratory for Optoelectronics, Huazhong University of Science and Technology, Wuhan, Hubei 430074, China

[Δ]Department of Mechanical & Materials Engineering, University of Nebraska-Lincoln, Lincoln, NE 68588, United States

[#]School of Optoelectronic Engineering and Instrumentation Science, Dalian University of Technology, Dalian, Liaoning 116023, China

[≠]Laser Micro/Nano-Fabrication Laboratory, School of Mechanical Engineering, Beijing Institute of Technology, Beijing 100081, China

*Address correspondence to: ylu2@unl.edu, dli8@unl.edu, weixiong@hust.edu.cn

[±]D.W. Li and C.Y.R. Wei contributed equally to this work.

ABSTRACT: The ability to design and enhance the nonlinear optical responses in two-dimensional (2D) transition metal dichalcogenides (TMDCs) is both of fundamental interest and highly desirable for developing TMDC-based nonlinear optical applications, such as nonlinear convertors and optical modulators. Here, we report for the first time a strong anisotropic enhancement of optical second-harmonic generation (SHG) in monolayer molybdenum disulfide (MoS_2) by integrating with one-dimensional (1D) titanium dioxide nanowires (NWs). The SHG signal from the MoS_2/NW hybrid structures is over two orders of magnitude stronger than that in the bare monolayer MoS_2. Polarized SHG measurements revealed a giant anisotropy in SHG response of the MoS_2/NW hybrid. The pattern of the anisotropic SHG depends highly on the stacking angle between the nanowire direction and the MoS_2 crystal orientation, which is attributed to the 1D NW-induced directional strain fields in the layered MoS_2. Similar effect has also been observed in bilayer MoS_2/NW hybrid structure, further proving the proposed scenario. This work provides an effective approach to selectively and directionally designing the nonlinear optical response of layered TMDCs, paving the way for developing high-performance, anisotropic nonlinear photonic nanodevices.

KEYWORDS: second-harmonic generation, anisotropic enhancement, transition metal dichalcogenides, 2D/1D hybrid, strain field

Advances in nonlinear optics (NLO) rely on the development of new device structures implementing novel materials with tailored optical properties. Two-dimensional (2D) transition metal dichalcogenides (TMDCs), such as molybdenum disulfide (MoS_2), have shown to exhibit numerous fascinating nonlinear optical behaviors, including second-harmonic generation (SHG),[1-3] sum-frequency generation,[4-5] third-harmonic generation,[6] four-wave mixing,[4, 7] and high-harmonic generation.[8] This makes them promising candidates for diverse emerging applications (*e.g.*, biomedical imaging, frequency conversion, terahertz light detection, attoscience, and nonlinear light modulators[8-12]). However, direct utilization of 2D TMDCs for NLO is still a great challenge due to the reduced light-matter interaction length at the atomic layer thickness scale and the poor field confinement, thus limiting nonlinear conversion efficiency. On the other hand, strong anisotropic NLO responses have recently been observed in some low-symmetry 2D materials, such as black phosphorus and rhenium disulfide,[13-16] while unstable nature of these materials in ambient conditions makes it not suitable for practical applications.[17-19] It is thus highly desirable to design and enhance the nonlinear optical response, such as SHG, in air-stable MoS_2 for angular-dependent nonlinear photonic devices, which has been challenging in the isotropic 2D TMDCs.[9, 20-24]

To date, various strategies have been developed to enhance the optical SHG process in 2D TMDCs. For example, SHG intensity can be strongly enhanced by orders of magnitude when the excitation photons are resonant with the exciton in 2D TMDCs.[22, 25] However, it might be interfered by the unwanted higher-order nonlinear optical signals, thus only allowing a very low pumping intensity.[26] The electrical control of SHG in a monolayer tungsten diselenide has also been demonstrated,[23] where the intensity of SHG from the resonant excitation of A exciton is tunable by over an order of magnitude at low temperature but by only a factor of four at room

temperature. Another approach to enhancing SHG signals is to combine 2D TMDCs with various plasmonic metasurfaces[20, 26-27] and optical structures (*e.g.*, waveguides[21, 28] and cavities,[29] *etc*). Although these hybrid structures can enhance the NLO signals in 2D TMDCs, the complicated fabrication processes are not suitable for manufacturing low-cost, efficient, nonlinear optical nanodevices.

Recently, dielectric nanowires (DNWs) have been demonstrated to be an ideal system for nanophotonic exploration due to their simple geometry and their ability to control the local density of optical states at the location of the emitter as well as the radiation pattern, thus allowing for efficiency enhancements and directional emissions.[30-31] As a result, DNWs have become a versatile tool for super-resolution imaging and directive nanophotonic lenses.[31-32] For NLO processes, integrating 2D TMDCs with one-dimensional (1D) nanowire structures provides an opportunity to realize directional and enhanced nonlinear optical emissions, which has barely been explored to date.

In this work, we report a 2D/1D TMDC/DNW hybrid structure that exhibits significantly enhanced and anisotropic SHG response compared with the bare TMDC layers. Li *et al.* first observed strong SHG intensity in monolayer MoS_2 due to the broken inversion symmetry, demonstrating it is an excellent candidate for SHG.[1] On the other hand, we used crystalline titanium dioxide (TiO_2) as a DNW material due to its high refractive index, low loss at visible wavelengths, as well as low cost. Here, monolayer MoS_2 flakes were selected and transferred on top of TiO_2 nanowires (Figure 1a). A combined experimental and numerical simulation study revealed that TiO_2 nanowire not only effectively increased the efficiency of the emitted SHG signal from monolayer MoS_2 by enhancing the local electric filed in the hybrid structure but also led to highly anisotropic SHG enhancement. In addition, the pattern of the anisotropic SHG response, as

a function of the stacking angle between the nanowire direction and the MoS_2 crystal orientation, has been established. The similar effect has also been observed in bilayer MoS_2/TiO_2 NW hybrid structure, which further proved our proposed scenario.

RESULTS AND DISCUSSION

To fabricate 2D/1D MoS_2/TiO_2 NW hybrid structure (Figure 1a), a suspension of TiO_2 nanowires was spin coated onto a clean silicon dioxide/silicon (SiO_2/Si) substrate. After drying, an exfoliated monolayer (1L) MoS_2 flake was transferred onto a selected TiO_2 nanowire under an optical microscopy. Figure 1b shows a false colored scanning electron microscopy (SEM) image of a hybrid structure, confirming that the MoS_2 flake (purple) was well integrated with the underneath TiO_2 nanowire (green). The topography of the 2D/1D hybrid was characterized by an atomic force microscopy (AFM) measurement, as shown in Figure 1c, where the TiO_2 nanowire had a small diameter of ~ 75 nm. Transmission electron microscopy (TEM), combined with the selected area electron diffraction (SAED) pattern analyses (Figure S1), indicated a single crystal rutile phase structure in TiO_2 nanowire along its entire length. The number of MoS_2 layers was determined using Raman and photoluminescence (PL) measurements (Figure S2). Cross-sectional high-resolution TEM (HR-TEM) measurements were carried out to further confirm the monolayer characteristic of MoS_2, the high crystallinity of TiO_2 nanowire, and the smooth interface between MoS_2 and TiO_2 nanowire (Figure 1d and Figure S3). More interestingly, we observed an air gap between MoS_2 and SiO_2/Si substrate (Figure 1d), indicating that a locally suspended MoS_2 layer formed on each side of the nanowire. This observation was consistent with the energy dispersive spectroscopy (EDS) mapping (Figure 1d) and the AFM measurements (Figure S4).

Then, we exploited the manipulation of SHG response from a 1L MoS_2/NW hybrid structure (Figure 2a). Figure 2b shows the corresponding SHG image as in Figure 2a, where the MoS_2 monolayer was partially coupled onto the TiO_2 nanowire with an average NW diameter of 100 nm (yellow dotted line). Clearly, the SHG emission from the 1L MoS_2 exhibited a weak signal, while the SHG emission from the hybrid structure exhibited a highly enhanced signal. Similar SHG enhancement was observed in more hybrid samples that we investigated (Figures S5a-c), suggesting that this is a highly reproducible phenomenon. We also noted that the enhanced SHG signals from the hybrid structure showed inhomogeneity (Figure 2b), which was attributed to the nonuniform diameter distribution in the same nanowire (Figure S6). This sensitive response to the nanowire diameter can be exploited for a controlled tuning of the SHG enhancement. Figure 2c shows the excitation power-dependent SHG for 1L MoS_2 without and with TiO_2 nanowires, corresponding to a slope value of ~ 2.1 and ~ 1.3, respectively. The expected quadratic power dependence of the SHG signal from the 1L MoS_2 further confirmed a second order nonlinear optical emission. Possible reasons for subquadratic power dependence in the hybrid structure can be attributed to the saturable absorption or phase match between the fundamental and second generated waves.[33] The enhanced SHG and promising saturable absorption properties in MoS_2/NW hybrid structures make them promising candidates for a wide range of applications in nonlinear optics.

To quantitatively estimate the SHG enhancement, we drew three profiles along the lines in Figure 2b and compared the SHG intensity of MoS_2 with and without the nanowire (Figure 2d). Both TiO_2 nanowire and SiO_2/Si substrate showed no observable SHG emission using a pump wavelength at 800 nm (green line), indicating that the enhanced SHG signal from the hybrid can only arise from the MoS_2. In addition, the SHG signal from the hybrid region was enhanced by

approximately 9 (orange line) to 12 (red line)-folds with respect to the bare 1L MoS_2. Considering the small area fraction of nanowires within the focused laser spot, we computed the maximum SHG enhancement factor ($EF_{\max}$) according to the formula:[34]

$$EF_{\max} = \frac{I_{\text{hybrid}}}{I_{MoS_2}} \cdot \frac{A_o}{A_{NW}}, \quad (1)$$

where I_{hybrid}, I_{MoS_2}, A_o, and A_{NW} are the SHG intensity of MoS_2 in the hybrid region, the SHG intensity of MoS_2 on SiO_2/Si substrate, the excitation area of the focused laser spot, and the area of the nanowire within the laser spot, respectively. According to this normalization method, the EF_{max} was calculated to be ~ 140.

It is also interesting to compare the linear optical responses of 1L MoS_2 and MoS_2/NW hybrid with their nonlinear optical responses. Figures 2a and S7a showed a weak optical signal scattered from the 1L MoS_2. In contrast, there was an obvious enhancement in the reflected optical signal from the TiO_2 nanowire regardless of the MoS_2 on top, which can be attributed to the effective light scattering properties of rutile phase TiO_2.[35] The difference between reflected light intensity from the sample on substrate and from the bare substrate can be quantified in terms of the image contract (C), which is defined as

$$C = \left|\frac{R_{sam} - R_{sub}}{R_{sub}}\right|, \quad (2)$$

[36-37]

where R_{sam} and R_{sub} represent the reflected signals from the sample and the substrate, respectively. By analyzing the optical reflection image (Figure S7a) using Equation (2), for 1L MoS_2 $C_{MoS_2} = 0.09$, while for MoS_2/NW hybrid $C_{MoS_2/NW} = 0.27$. Thus, the ratio of the linear optical signal from 1L MoS_2/NW to that from 1L MoS_2 ($C_{MoS_2/NW}/C_{MoS_2}$) was estimated to be ~ 3, much smaller than SHG nonlinear optical response ratio (~ 10). In addition, the scattered Raman and PL characterizations show that both signals from the MoS_2/NW are not enhanced but slightly

suppressed compared to the bare MoS_2 (Figure S2), which is probably due to the TiO_2 NW-induced linear absorption effect. The above analyses suggest the complicated and different enhancement mechanisms for linear and nonlinear optical responses in MoS_2/TiO_2 NW hybrids.

Subsequently, we quantitatively investigated the SHG enhancement mechanism for 1L MoS_2 integrated with a dielectric nanowire. Based on the symmetry of the MoS_2 monolayers, the SHG signal can be expressed as

$$I_{SHG} \propto |\boldsymbol{P}_{2\omega}|^2 = \left|\boldsymbol{\chi}^{(2)}_{MoS_2} : \boldsymbol{E}_{\omega} \cdot \boldsymbol{E}_{\omega}\right|^2,^{25} \quad (3)$$

where $\boldsymbol{P}_{2\omega}$ is the second-order polarization, $\boldsymbol{\chi}^{(2)}_{MoS_2}$ is the nonlinear susceptibility, and $\boldsymbol{E}_{\omega}$ is the incident electric field. According to Equation (3), the SHG intensity is proportional to the square of both the nonlinear susceptibility and the incident light intensity. In our case, considering no detectable SHG signal from the TiO_2 nanowire, the influence of nanowire-induced change in $\boldsymbol{\chi}^{(2)}_{MoS_2}$ on SHG enhancement was negligible. Thus, the enhanced SHG was considered to mainly result from a 1D nanowire-induced, localized, concentrated electric field in the 2D/1D hybrid, as well evidenced by the following numerical simulations. We modeled the electric field distributions inside the MoS_2/NW hybrid structure and the bare MoS_2 on SiO_2/Si substrate by finite-difference time domain (FDTD) simulations in a two-dimensional geometry. In the simulation, the diameter of the TiO_2 NW was set to be 100 nm, and the 1L MoS_2 was treated as a 1-nm-thick thin film. The refractive indices of the air, TiO_2 nanowire, MoS_2 film, and SiO_2 substrate were set to be 1, 2.79, 4.73 and 1.45, respectively. Figure 2e shows the electric field intensity distribution in the 1L MoS_2/NW hybrid structure under the excitation of a fundamental wave ($\lambda = 800$ nm). Interestingly, the light is effectively concentrated on both sides of the 2D/1D hybrid, but not in the core of the TiO_2 nanowire or at the interface between MoS_2 top layer and TiO_2 nanowire. The

largest electric field intensity ($|E|^2$) in the hybrid (Figure 2e) is enhanced by ~ 3.8 compared with that in the bare MoS_2 on the SiO_2/Si substrate (Figure 2f), suggesting the significantly enhanced light-matter interaction in the hybrid. It is known that the SHG intensity exhibits a 4th-order dependence on the electric field ($|E|^4$).[38] As a result, the calculation indicates that the SHG intensity can be enhanced by ~ 10 on average. When the laser beam size and NW diameter were accounted, the maximum SHG enhancement factor ($EF_{\max}$) was calculated to be ~ 130, which agrees well with the experimental result. On the other hand, similar to the reported PL enhancement in the freestanding TMDCs,[39] the suspended MoS_2 layers formed on each side of the nanowire (Figure 1d) also contributed a lot to the enhancement of SHG conversion efficiency because the substrate-induced doping and dielectric screening effects were eliminated. Here, the doping may come from substrate-borne water moisture and the substrate itself,[39] and the substrate screening may reduce the electron hole interaction, leading to a reduction in SHG.[40-41]

To gain a further understanding of the NLO engineering in 1L MoS_2 induced by the TiO_2 NWs, we carried out polarized SHG measurements (Figure 3a). A femtosecond (fs) laser with a central wavelength of 800 nm was linearly polarized and focused onto the samples, with the analyzer set parallel to the incident light polarization. The SHG polar intensity distributions were obtained by rotating the sample through 360° in 10° steps for configuration. We first confirmed the crystal orientations of the MoS_2 in three different hybrid samples (Figures S5d-f),[1-2, 42] from which the stacking angle (θ) between the NW direction and the MoS_2 crystalline orientation was determined (Figure 3b).

Figure 3c presents the polarization-resolved SHG signal from a hybrid with nanowire along the armchair (AC) direction of the MoS_2 ($\theta = 0^o$). The angular dependence of the SHG from 1L MoS_2 (red curve) exhibited a characteristic six-fold rotational symmetry, with an SHG intensity changes

as $I_{MoS_2}^{SHG} \propto cos^2 3(\varphi + \varphi_0)$, where φ is the sample rotation angle, and φ_0 $(= 0^o)$ is the offset angle between the armchair axis of MoS_2 and the incident laser polarization. Interestingly, the polarization-resolved, enhanced SHG emission from the hybrid region (blue curve) no longer followed the six-fold symmetry polarization pattern. The signal started with a maximum value at $\varphi = 0^o$ and fell to a minimum value when $\varphi = 90^o$. This clearly indicates that the SHG response from the hybrid structure can be modulated directionally. In addition, the SHG pattern behavior can be described by a modified model used for 2D TMDC strain analysis:[43]

$$I_{MoS_2/NW}^{SHG} = (\mathrm{A}cos3(\varphi + \varphi_0) + \mathrm{B}cos^3(\varphi + \varphi_0) - \mathrm{C}sin^3(\varphi + \varphi_0)\cos(\varphi + \varphi_0))^2 + I_0, \quad (4)$$

where $\varphi_0 = 0^o$, I_0 is the minimum SHG intensity which is independent of φ,[44-45] A, B, and C are three constants related to the tensor elements of the hybrid structure. Using this model, we can extract the fitting parameters for A, B, and C (Table S1). In our case, the first term represents the influence of the MoS_2 crystal orientation, and the latter two terms reflect how nanowire influences the SHG intensity distribution. To quantatively understand the anisotropy in SHG response, we obtained the pattern of the enhancement factor by comparing the polarized SHG intensity from hybrid with that from 1L MoS_2 (Figure 3f), which showed a strong angular dependence. The enhancement factor reached to a maximum value ($EF_{max} \approx 30$) at $\varphi = 30^o$ (210^o) and 150^o (330^o) (along two zigzag (ZZ) axes), a submaximal value ($EF_{submax} \approx 8$) when $\varphi = 0^o$ (180^o) (along the NW direction), and a minimum value ($EF_{min} \approx 5$) at $\varphi = 90^o$ (270^o) (perpendicular to the NW direction).

We then investigated the polarization-resolved SHG emission from a hybrid sample with nanowire along the ZZ direction of MoS_2 ($\theta = 30^o$) (Figure 3d), where SHG intensity was minimum when $\varphi = 0^o$ and reached maximum when $\varphi = 90^o$ (blue curve). Furthermore, the

correpsonding SHG EF pattern (Figure 3g) showed an obviously different angular dependence compared to that with $\theta = 0^o$, which achieved a maximum value at $\varphi = 60^o$ $(120^o, 240^o, 300^o)$, a submaximal value at $\varphi = 90^o$ (270^o), and a minimum value at $\varphi = 0^o$ (180^o). To better understand the SHG pattern evolution, we also fabricated a MoS_2/NW hybrid structure with nanowire neither along the AC nor ZZ direction ($\theta \approx 12^o$) (Figure S5f). In this case, the influence of nanowire on the anisotropic SHG response was more obvious in comparison with the other two cases ($\theta \approx 0^o, 30^o$), where the polarized SHG pattern from the hybrid had the same tendency as that of the bare MoS_2 monolayer, both showing a six-fold symmetry (Figure 3e); while the SHG enhancement factor exhibited maximum (minimum) values along three ZZ (AC) axes of MoS_2 (Figure 3h). To confirm the change in SHG enhancement pattern from $\theta = 0^o$ to 30^o is invariant to NW position, we carried out polarized SHG measurements at different locations along the NW for the samples in Figures S7d-f (see Supplementary Figures S8, S9 and S10). The above analyses, revealing a highly anisotropic SHG enhancement in MoS_2 by integrating with 1D NWs, indicate a strong dependence of the observed effect on the stacking angle between the NW direction and the MoS_2 crystal orientation.

The anisotropic SHG enhancement is elaborated below. According to previous reports, the polarization dependence of SHG intensity is very sensitive to the lattice symmetry of MoS_2.[2, 43] In addition, the enhanced SHG in 1L MoS_2 on the flat thin films showed no polarization dependence (data not shown), namely, the exhibiting of isotropic SHG enhancement. Thus, the symmetry breaking in the SHG polarization pattern as well as the anisotropic SHG enhancement observed in Figure 3 was attributed to the 1D NW-induced crystal lattice deformation, which broke the three-fold crystal symmetry of MoS_2. A closer examination of the AFM topography (Figure S4) suggests that the 2D/1D geometry induced a maximum strain, ε of ~ 0.1%, in the MoS_2 on top. Due to such

a small strain value, there were no obvious changes in the Raman/PL peak positions shift; only a little decrease in the peak intensity of 1L MoS_2 was found (Figure S2). It indicates that the SHG is very sensitive to the strain amplitude in the 2D TMDCs, consistent with previous reports.[43, 46]

To understand why different anisotropic SHG enhancement behaviors were observed in the three hybrid samples discussed above, we established an analysis model (Figure 4). As shown in Figure 4a, the MoS_2 layer was locally stretched along the vertical direction of nanowire (black arrow) due to the transfer, which caused the MoS_2 to be tensilely and compressively strained perpendicular (blue arrow) and parallel (pink arrow) to the nanowire, respectively. Theoretical studies indicate a highly anisotropic mechanical response in 2H-MoS_2, namely, the bond lengths and bond angles, *etc*., respond differently to strains along the ZZ and AC directions.[47] For example, the uniaxial deformation along the ZZ direction has much larger ultimate strains than that along the AC direction.[48] Peng *et al.* reported that ZZ nanoribbons are softer and have larger tolerance to the strains than AC nanoribbons, indicating a higher chemical bond change rate along the ZZ direction than along AC direction.[47] Therefore, the degree of the variation in the lattice structure of MoS_2 under ZZ axis strain is larger than that under AC axis strain.

It is noted that the SHG intensity in 2D TMDCs decreased linearly as the strain increased,[43] which can be explained by the strain-induced modification of the nonlinear susceptibility tensor due to a photoelastic effect.[46] In our case, the tensile and compressive strain fields applied to MoS_2 were determined by the 1D NWs. When the NW was along the AC direction ($\theta = 0^{o}$), ZZ axis (tensile) strain-induced deformation in MoS_2 was larger than AC axis (compressive) strain-induced deformation (Figure 4b), thus leading to SHG enhancement factor perpendicular to NW ($EF_{\perp NW}$) smaller than that parallel to NW ($EF_{\parallel NW}$). While for the NW along the ZZ direction ($\theta = 30^{o}$), the AC axis (tensile) strain only induced a small atomic displacement compared to that by the

(compressive) strain along the ZZ axis (Figure 4c), which resulted in $EF_{\perp NW} > EF_{\parallel NW}$. In the case of NW along the arbitrary direction ($\theta \neq 0^o, 30^o$), the strain field distribution in MoS_2 became more complex but was expected to generate quasi-isotropic in-plane deformation with a stacking angle θ close to 15° (Figure 4d), corresponding to $EF_{\perp NW} \approx EF_{\parallel NW}$. Thus, it can be concluded that the 1D NW-induced strain fields in MoS_2 depend on the MoS_2/NW stacking angle, thereby explaining the different anisotropic SHG enhancement behaviors in three MoS_2/NW hybrid structures. Moreover, the polarization dependence of the SHG enhancement factor can be developed as a reliable approach for determining the local strain field in a 2D/1D hybrid.

To further enhance the SHG efficiency as well as prove and exploit our findings in MoS_2 monolayers, we extended our investigation to the twisted bilayer MoS_2/NW hybrid structures. Recent advances in twisted van der Waals homo- and hetero-structures have provided a new route to tailoring the physical properties of 2D TMDCs.[45, 49-51] As an example, the SHG signal of TMDC bilayers can be enhanced by ~ 4 times compared to that of individual monolayers with precise control of the twist angles.[45]

Figure S11a shows the optical image of a twisted bilayer MoS_2/TiO_2 NW hybrid structure, which was fabricated by deterministic transfer. The isolated MoS_2 monolayer (Region A and Region B) and bilayer (Region C) were first studied by the polarized SHG, from which the crystal orientation of each monolayer and the stacking angle of the bilayer were determined (Figure S11). In our polarization measurement, the incident laser was linearly polarized along the *x*-axis, which was aligned with the horizontal direction of the TiO_2 nanowire (see inset in Figure S11a). The SHG from all three regions exhibited a six-fold pattern (Figures S11b-d), where the zigzag axis of Region A and the armchair axis of Region B were parallel to the horizontal direction of the nanowire, indicating the formation of a bilayer with a twisted angle of ~ 30° at Region C. Further,

the presence of inversion symmetry breaking at Region C (Figure S11d) suggested that the stacked MoS_2 bilayer belonged to the noncentrosymmetric D_{3h} point group, thus allowing significant second order nonlinear optical response (Figures 5a and S12). More interestingly, the polarized SHG intensity maximum from Region C lies along a direction between two 1L MoS_2 flakes (Figure S11d), which we defined as the crystal orientation of the MoS_2 bilayer. We were able to explain this effect quantitatively *via* point group symmetry (see Supplementary Note 1 for details). Here, a linear combination of components of two 1L MoS_2 nonlinear susceptibility tensors, $\boldsymbol{\chi}_C^{(2)} = \boldsymbol{\chi}_B^{(2)} + \boldsymbol{\chi}_A^{(2)}$ (Figure 5b), was used to obtain polarization-dependent SHG response from Region C:

$$I_C^{2\omega}(\varphi) = C\left|d_{MoS_2}\right|^2 |cos3(\varphi - 15)|^2, \quad (5)$$

where d_{MoS_2} is the tensor element, and φ is the polarization angle of the incident light. Using our SHG model, we fitted the experimental data, as shown in Figure S11. The fitting of Region C using Equation (5) agreed well with the experimental data, indicating that the crystal orientation of bilayer MoS_2 was rotated by ~ 15^o with respect to the horizontal direction of the nanowire, namely, $\theta \approx 15^o$.

Figure 5a shows the corresponding SHG image as in Figure S11a, where the SHG signals from the MoS_2 bilayer and bilayer MoS_2/NW hybrid were both approximately two times stronger than those of the individual 1L MoS_2 and 1L MoS_2/NW hybrid. This result is in good agreement with our SHG modeling (see Supplementary Note 1). As shown in Figures 5c and 5d, the polarized SHG intensity values from the two 1L MoS_2/NW hybrid structures exhibited asymmetric six-fold patterns, corresponding to different patterns of the SHG enhancement factor (Figure S13), which further confirmed a close relationship between the SHG enhancement anisotropy and the MoS_2/NW stacking angle. Figure 5e (left panel) displays a six-fold SHG symmetry pattern for the

bilayer MoS_2/NW hybrid with $\theta \approx 15^o$, which is consistent with that of the twisted MoS_2 bilayer (Figure S11d). The corresponding SHG EF pattern (right panel in Figure 5e) exhibits similar polarization dependent behavior to that was observed in 1L MoS_2/NW hybrid with $\theta \approx 12^o$ (Figure 3h), showing an EF maximum (minimum) when the incident laser polarization aligns with the ZZ (AC) direction of bilayer MoS_2. This indicates that our findings are general and applicable to any other noncentrosymmetric van der Waals materials.

CONCLUSIONS

In summary, we designed a unique 2D/1D MoS_2/TiO_2 NW hybrid structure to realize significant improvement in nonlinear optical conversion efficiency. The SHG emission from the hybrid structure exhibits more than two orders of magnitude enhancement compared with that of the bare MoS_2 on SiO_2/Si substrate. The SHG enhancement was attributed to the intensification of the local electric field in the hybrid structure due to strong light-matter coupling and the suspension of the MoS_2 without the substrate-induced doping and dielectric screening effects. In addition, the SHG can be effectively controlled by varying the polarization of the incident light, leading to anisotropic SHG enhancement. One-dimensional NW-induced crystal lattice deformation is a key factor that leads to strong anisotropic SHG enhancement in atomically layered MoS_2. This method can be exploited to manipulate many other nonlinear optical processes, such as third-harmonic generation and high-harmonic generation, in 2D TMDCs. Our work thus provides a new and simple platform for selectively and directionally designing nonlinear optical responses in 2D layered TMDCs for developing cost-effective, high-efficiency, anisotropic nonlinear optical nanodevices.

METHODS

Fabrication of 2D/1D MoS_2/TiO_2 NW hybrid structures. The MoS_2/TiO_2 NW hybrid structures were fabricated by a dry transfer technique, which included the following four steps:

1) TiO_2 nanowires were dispersed in ethanol solution by sonication and then spin coated onto the SiO_2(300 nm)/Si substrates.

2) 1L MoS_2 flakes were prepared by mechanical exfoliation from the bulk crystals (Graphene Supermarket) with Scotch™ tape and then transferred onto gel-film coated glass slides.

3) To realize the integration of monolayer MoS_2 with TiO_2 nanowire in a precisely controlled twist angle, the monolayer characteristic of as-exfoliated MoS_2 flakes on gel films were confirmed by combining optical contrast and Raman measurements. Meanwhile, their crystalline orientations were determined by the polarization-dependent SHG measurements.

4) The 1L MoS_2 flake on top of gel film was aligned with the TiO_2 nanowire on SiO_2/Si substrate under an optical microscope system, in contacted with each other. Then the two substrates were slowly separated, forming 1L MoS_2/TiO_2 NW hybrid structure. We also fabricated a stacked bilayer MoS_2/NW hybrid structure by transferring another 1L MoS_2 flake onto a 1L MoS_2/NW hybrid on SiO_2/Si substrate.

SHG measurements. The SHG measurements were conducted using a homemade multiphoton nonlinear optical microscopy system as previously described.[4] In brief, a commercial fs laser

(MaiTai® DeepSee™ HP, SpectraPhysics) with a center wavelength of 800 nm was used as an excitation light source. We focused a fs laser beam onto the sample through a 25× magnification water-immersion objective and collected SHG signals in the backward direction by a photomultiplier tube (PMT). The polarized SHG measurements were performed by fixing both the polarizer and analyzer (with analyzer parallel to the polarization of incident light) and rotating the samples with 10-degree steps.

Other characterizations. Raman and photoluminescence measurements were conducted on a micro-Raman system (Renishaw InVia™ Plus, Renishaw, Gloucetershire, U.K.) under an ambient environment, where an Ar^+ laser with a wavelength of 514.5 nm and a power of ~ 1.5 mW was used as an excitation laser source. Atomic force microscopy measurements were carried out in a Bruker MultiMode 8 AFM system using a tip (ScanAsyst® AIR, Bruker Nano Inc., U.S.A.) working with peak-force tapping mode. Transmission electron microscopy and HR-TEM images were acquired using a fully digital 200 kV TEM system (Tecnai Osiris™ scanning, FEI, U.S.A.) equipped with a super-X windowless EDS detector and a HAADF detector. The MoS_2/NW hybrid samples for cross-sectional TEM imaging were prepared by a standard focused ion beam (FIB) lift-out technique within a chamber of a FIB-SEM system (Thermo Scientific™ Helios NanoLab™ 660, FEI, U.S.A.).

ACKNOWLEDGEMENTS

This research was financially supported by the National Science Foundation (CMMI 1826392), Office of Naval Research (N00014-15-C-0087), the National Natural Science Foundation of China (61774067, 51145237, U1609209), the National Key R&D Program of China (2017YFB1104300), the Nebraska Center for Energy Science Research, and the Fundamental Research Funds for the Central Universities (HUST:2018KFYXKJC027). Work by J.S. and X.H.

was supported by the U.S. Department of Energy (DOE), Office of Science, Basic Energy Sciences (BES), under Award No. DE-SC0016153 (scanning probe studies).

ASSOCIATED CONTENT

Supporting Information available: The Supporting Information is available free of charge on the ACS Publications website at http://pubs.acs.org.

TEM, Raman, PL, EDS, and AFM characterizations, identification of monolayer and bilayer MoS_2 crystal orientations, the patterns of SHG enhancement factor, and modeling of SHG in twisted bilayer MoS_2.

AUTHOR CONTRIBUTIONS

D.L. and Y.L. conceived the idea and designed the experiments. D.L. and C.W. prepared the MoS_2/NW hybrid samples and performed the SHG measurements. D.L. and X. Huang modeled the SHG signals and performed the FDTD simulation studies. J.S. and X. Hong carried out the AFM studies. F.W. and B.C. carried out the TEM characterizations. D.L., W.X. and L.J. carried out the PL studies. D.L., K.L. and A.F. carried out Raman characterizations. D.L. and C.W. wrote the manuscript. All authors commented on the manuscript.

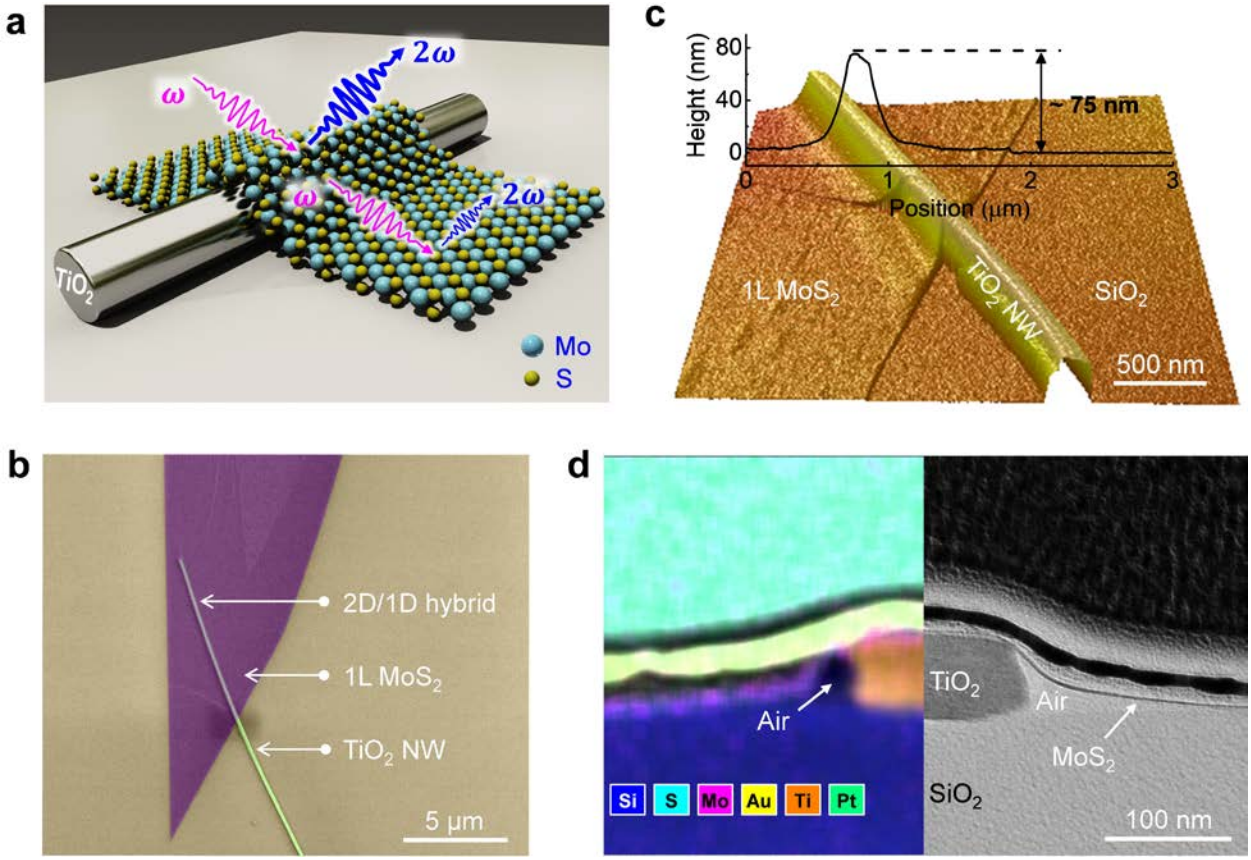

Figure 1. Characterization of 2D/1D MoS_2/TiO_2 NW hybrid structure. (a) Schematic of a monolayer (1L) MoS_2 integrated with single TiO_2 nanowire and irradiated by the fundamental wave (ω), where backscattered SHG signal (2ω) was collected. (b) False colored SEM image and (c) AFM topography of a 1L MoS_2/NW hybrid structure on SiO_2/Si substrate. Inset in (c) shows the corresponding height profile. (d) Cross-sectional HR-TEM image (right) and overlapped energy-dispersive X-ray spectrometry mapping (left) for the same sample as in (b).

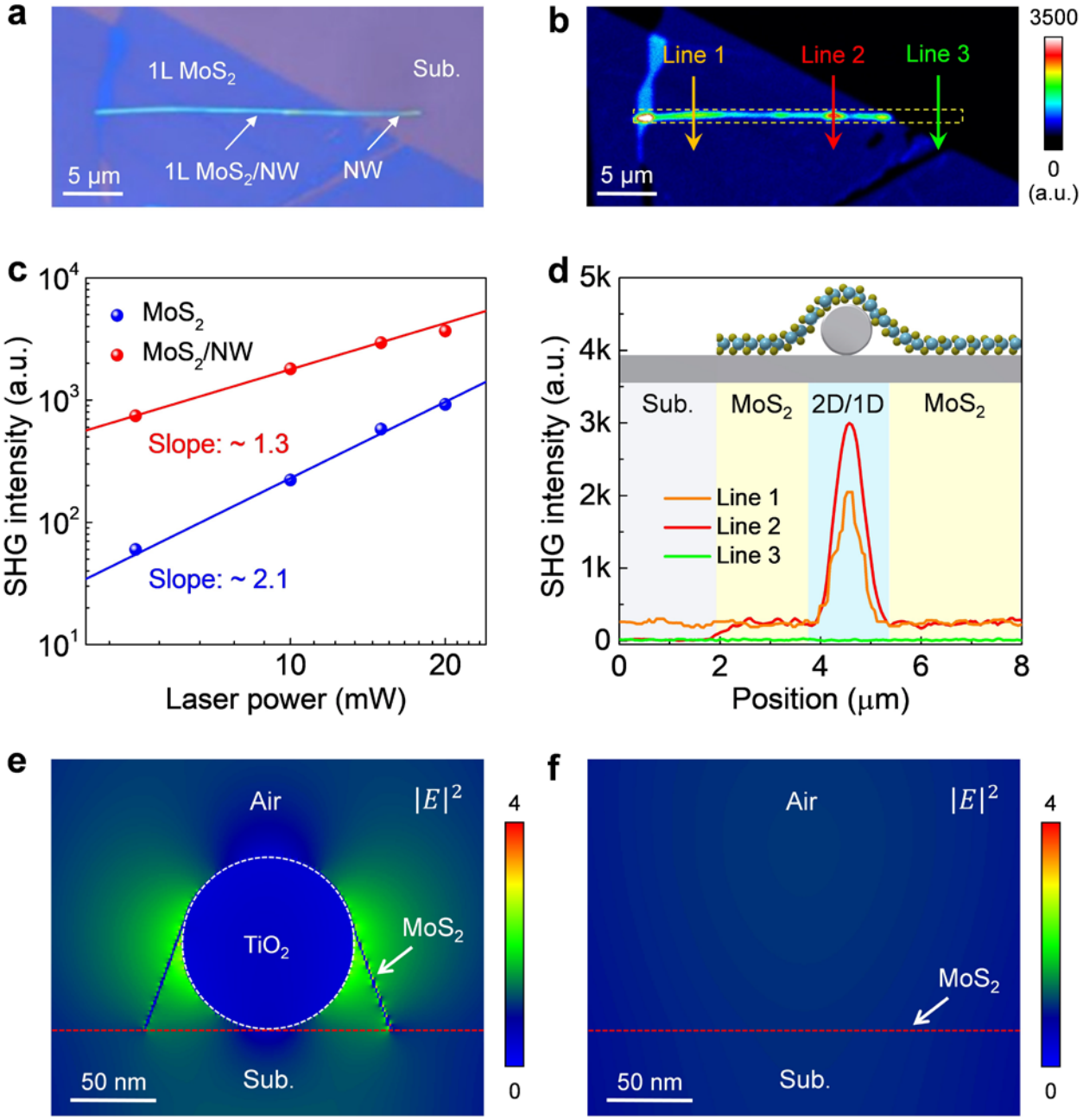

Figure 2. SHG enhancement from the 1L MoS_2/TiO_2 NW hybrid structure. (a) Optical image of a 1L MoS_2/NW hybrid on a SiO_2/Si substrate with (b) the corresponding SHG image. The color scale bar represents SHG intensity. (c) SHG intensity from the 1L MoS_2 (blue) and 1L MoS_2/NW hybrid (red) as a function of the excitation laser power. The dots are experimental data with the fits in solid lines. (d) SHG intensity profiles along the lines in (b). Top inset: schematic side view

of a 1L MoS_2/NW hybrid on SiO_2/Si substrate. (e,f) Calculated electric field distribution ($|E|^2$) excited by the fundamental wave ($\lambda = 800$ nm) in the (e) MoS_2/NW hybrid and (f) bare MoS_2 film on SiO_2/Si substrate. The dashed red and white lines donate the SiO_2 interlayer and the edge of TiO_2 NW, respectively.

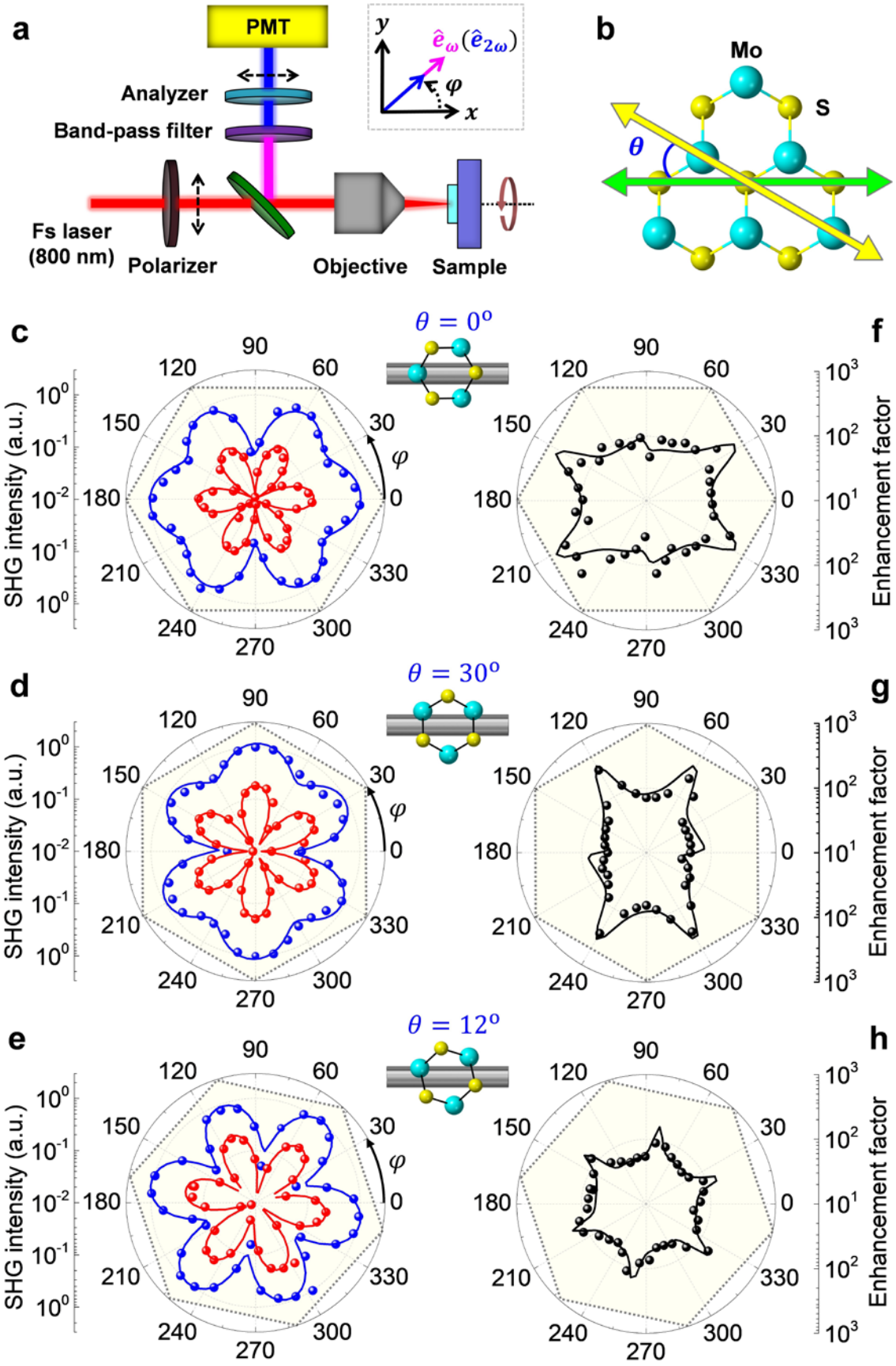
a
PMT
Analyzer
Band-pass filter
Fs laser
(800 nm)
Polarizer
Objective
Sample
$\hat{e}_\omega(\hat{e}_{2\omega})$
φ
b
Mo
S
θ
c
$\theta = 0^o$
d
$\theta = 30^o$
e
$\theta = 12^o$
f
g
h
SHG intensity (a.u.)
Enhancement factor

Figure 3. Anisotropic SHG enhancement in 1L MoS_2 by integrating with TiO_2 NW. (a) The schematic setup for polarized SHG measurements. Inset: φ in the laboratory coordinate is the rotation angle of the sample and only parallel component of SHG signal is measured. (b) Top view of the MoS_2 crystal orientation (yellow arrow) with respect to the horizontal direction of NW (green arrow). θ is the stacking angle between NW direction and MoS_2 crystal orientation. (c-e) Polar plots of the parallel polarization SHG intensity from the 1L MoS_2 (red) and the 1L MoS_2/NW hybrid (blue) as a function of the sample rotation angle normalized to the maximum SHG intensity of the 1L MoS_2/NW hybrid under three different stacking angles θ: (c) 0° (NW along AC direction), (d) 30° (NW along ZZ direction), and (e) ~12° (NW along neither AC nor ZZ direction). (f-h) The corresponding patterns of SHG enhancement factor for the samples in (c-e). The dots and solid lines are the experimental data and theoretical fitting, respectively. Zero degree in all plots is set along the NW direction. Insets in (c-h): top views of 1L MoS_2 integrated with TiO_2 NW, showing corresponding orientations.

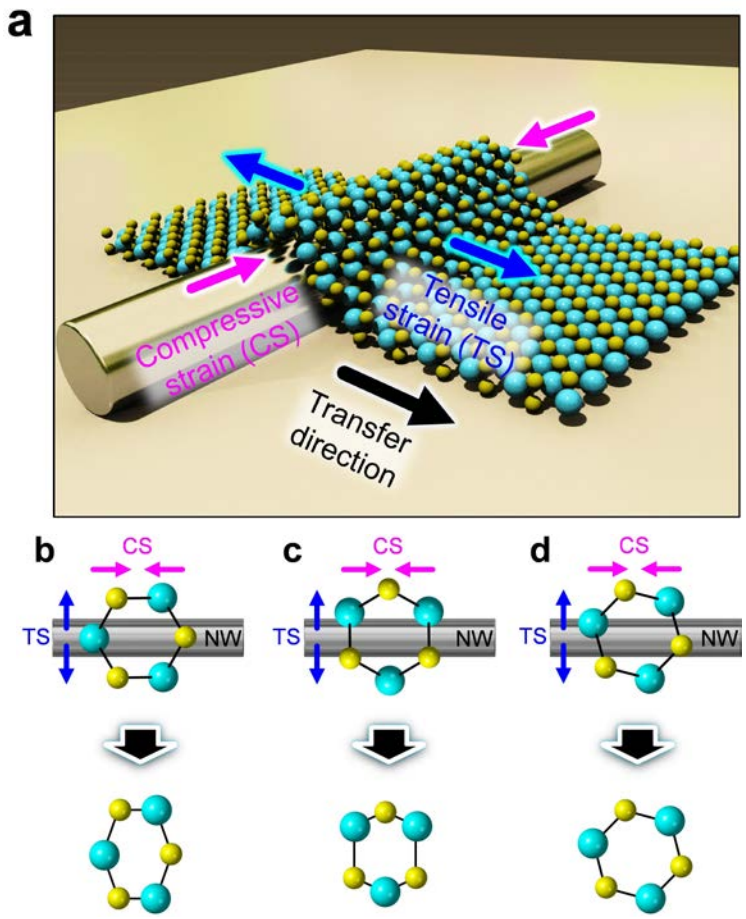

Figure 4. 1D NW-induced lattice deformation in 1L MoS_2. (a) Schematic of local strain formed in 1L MoS_2 due to transfer, where the tensile strain is applied perpendicular to the NW direction (blue arrows); and the compressive strain is induced along the NW direction (pink arrows). (b-d) Top views of MoS_2 crystal orientation with respect to the NW direction (upper panel) and the corresponding distorted lattice structures under tensile/compressive strains along two directions (bottom panel). The deformation ratio along two lattice directions is determined by the MoS_2/NW stacking angles.

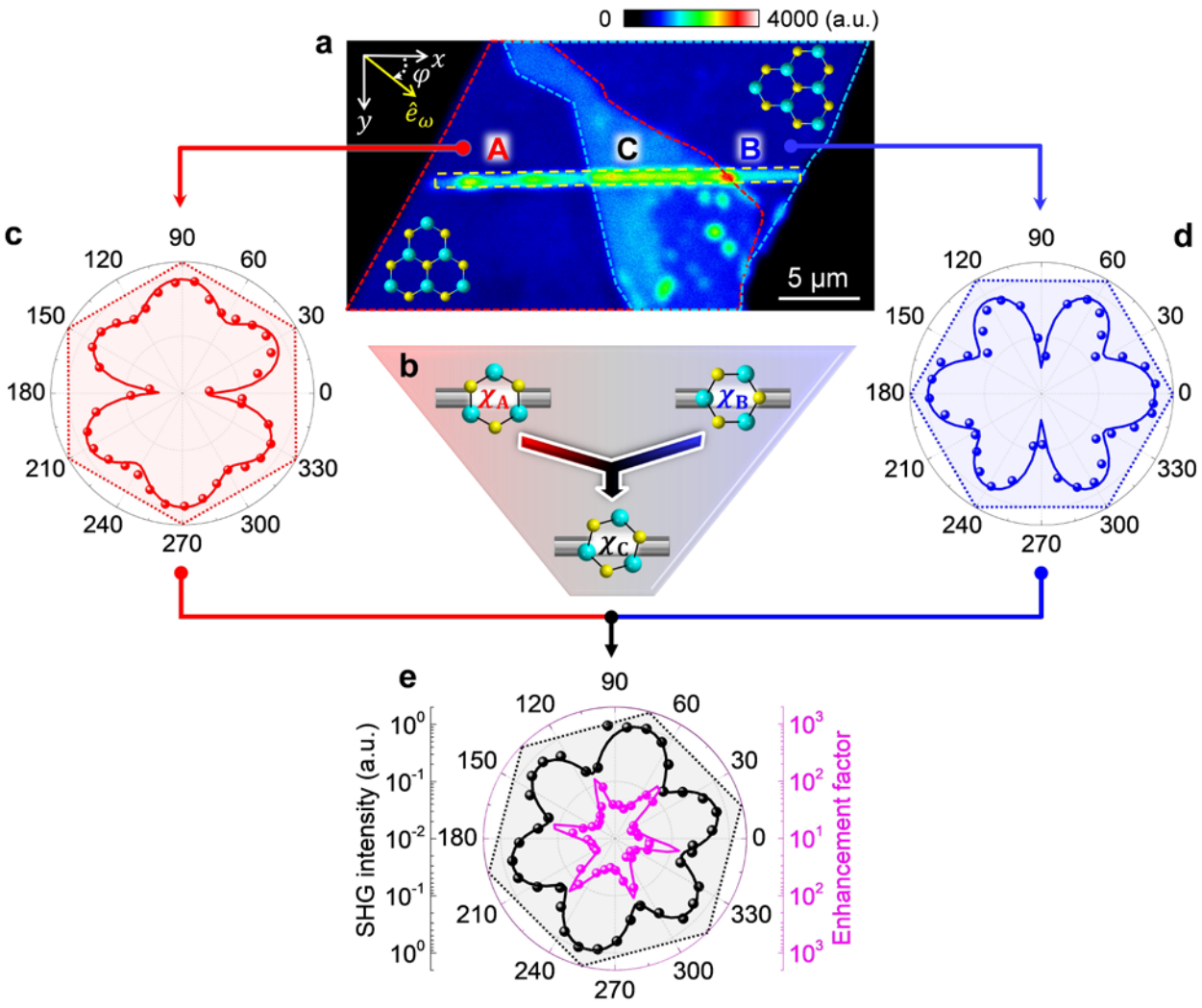

Figure 5. Anisotropic SHG enhancement from the twisted bilayer MoS_2/TiO_2 NW hybrid structure. (a) SHG image of a stacked bilayer MoS_2 (Region C) with twisting angle of ~ 30° integrated with a underneath TiO_2 nanowire on SiO_2/Si substrate. The dashed lines in yellow, red and blue outline the TiO_2 nanowire and 1L MoS_2 for Region A and Region B, respectively. The crystal orientation of 1L MoS_2 for each region is shown in (a) inset. The color scale bar represents SHG intensity. (b) A schematic showing the relationship of nonlinear susceptibility tensor among three regions: $\chi_C^{(2)} = \chi_B^{(2)} + \chi_A^{(2)}$. (c-d) Polar plots of the parallel polarization SHG intensity as a function of the sample rotation angle obtained from the 1L MoS_2/NW hybrids in (c) Region A and (d) Region B. (e) The patterns of (left) parallel polarized SHG intensity and (right) corresponding

SHG enhancement factor from the twisted bilayer MoS_2/NW hybrid. The dots and solid lines in (c-e) are the experimental data and theoretical fits, respectively.

REFERENCES

1. Li, Y.; Rao, Y.; Mak, K. F.; You, Y.; Wang, S.; Dean, C. R.; Heinz, T. F. Probing Symmetry Properties of Few-Layer MoS_2 and H-BN by Optical Second-Harmonic Generation. *Nano Lett.* **2013,** *13*, 3329-3333.
2. Malard, L. M.; Alencar, T. V.; Barboza, A. P. M.; Mak, K. F.; de Paula, A. M. Observation of Intense Second Harmonic Generation from MoS_2 Atomic Crystals. *Phys. Rev. B* **2013,** *87*, 201401.
3. Lin, K.-Q.; Bange, S.; Lupton, J. M. Quantum Interference in Second-Harmonic Generation from Monolayer WSe_2. *Nat. Phy.* **2019**, 1.
4. Li, D.; Xiong, W.; Jiang, L.; Xiao, Z.; Rabiee Golgir, H.; Wang, M.; Huang, X.; Zhou, Y.; Lin, Z.; Song, J.; Ducharme, S.; Jiang, L.; Silvain, J.-F.; Lu, Y. Multimodal Nonlinear Optical Imaging of MoS_2 and MoS_2-Based Van Der Waals Heterostructures. *ACS Nano* **2016,** *10*, 3766-3775.
5. Li, D.; Xiao, Z.; Mu, S.; Wang, F.; Liu, Y.; Song, J.; Huang, X.; Jiang, L.; Xiao, J.; Liu, L.; Ducharme, S.; Cui, B.; Hong, X.; Jiang, L.; Silvain, J.-F.; Lu, Y. A Facile Space-Confined Solid-Phase Sulfurization Strategy for Growth of High-Quality Ultrathin Molybdenum Disulfide Single Crystals. *Nano Lett.* **2018,** *18*, 2021-2032.
6. Wang, R.; Chien, H.-C.; Kumar, J.; Kumar, N.; Chiu, H.-Y.; Zhao, H. Third-Harmonic Generation in Ultrathin Films of MoS_2. *ACS Appl. Mater. Interfaces* **2013,** *6*, 314-318.
7. Jakubczyk, T.; Delmonte, V.; Koperski, M.; Nogajewski, K.; Faugeras, C.; Langbein, W.; Potemski, M.; Kasprzak, J. Radiatively Limited Dephasing and Exciton Dynamics in $MoSe_2$ Monolayers Revealed with Four-Wave Mixing Microscopy. *Nano Lett.* **2016,** *16*, 5333-5339.

8. Liu, H.; Li, Y.; You, Y. S.; Ghimire, S.; Heinz, T. F.; Reis, D. A. High-Harmonic Generation from an Atomically Thin Semiconductor. *Nat. Phys.* **2017,** *13*, 262.

9. Autere, A.; Jussila, H.; Dai, Y.; Wang, Y.; Lipsanen, H.; Sun, Z. Nonlinear Optics with 2D Layered Materials. *Adv. Mater.* **2018**, 1705963.

10. Dai, W.; Dong, H.; Fugetsu, B.; Cao, Y.; Lu, H.; Ma, X.; Zhang, X. Tunable Fabrication of Molybdenum Disulfide Quantum Dots for Intracellular Microrna Detection and Multiphoton Bioimaging. *Small* **2015,** *11*, 4158-4164.

11. Huang, Y.; Zhu, L.; Zhao, Q.; Guo, Y.; Ren, Z.; Bai, J.; Xu, X. Surface Optical Rectification from Layered MoS_2 Crystal by THZ Time-Domain Surface Emission Spectroscopy. *ACS Appl. Mater. Interfaces* **2017,** *9*, 4956-4965.

12. Schaibley, J. R.; Yu, H.; Clark, G.; Rivera, P.; Ross, J. S.; Seyler, K. L.; Yao, W.; Xu, X. Valleytronics in 2D Materials. *Nat. Rev. Mater.* **2016,** *1*, 16055.

13. Rodrigues, M. J.; de Matos, C. J.; Ho, Y. W.; Peixoto, H.; de Oliveira, R. E.; Wu, H. Y.; Neto, A. H. C.; Viana-Gomes, J. Resonantly Increased Optical Frequency Conversion in Atomically Thin Black Phosphorus. *Adv. Mater.* **2016,** *28*, 10693-10700.

14. Autere, A.; Ryder, C. R.; Säynätjoki, A.; Karvonen, L.; Amirsolaimani, B.; Norwood, R. A.; Peyghambarian, N.; Kieu, K.; Lipsanen, H.; Hersam, M. C. Rapid and Large-Area Characterization of Exfoliated Black Phosphorus Using Third-Harmonic Generation Microscopy. *J. Phys. Chem. Lett.* **2017,** *8*, 1343-1350.

15. Song, Y.; Hu, S.; Lin, M.-L.; Gan, X.; Tan, P.-H.; Zhao, J. Extraordinary Second Harmonic Generation in ReS_2 Atomic Crystals. *ACS Photonics* **2018,** *5*, 3485-3491.

16. Cui, Q.; Muniz, R. A.; Sipe, J.; Zhao, H. Strong and Anisotropic Third-Harmonic Generation in Monolayer and Multilayer ReS_2. *Phys. Rev. B* **2017,** *95*, 165406.

17. Favron, A.; Gaufrès, E.; Fossard, F.; Phaneuf-L'Heureux, A.-L.; Tang, N. Y.; Lévesque, P. L.; Loiseau, A.; Leonelli, R.; Francoeur, S.; Martel, R. Photooxidation and Quantum Confinement Effects in Exfoliated Black Phosphorus. *Nat. Mater.* **2015,** *14*, 826.

18. Wood, J. D.; Wells, S. A.; Jariwala, D.; Chen, K.-S.; Cho, E.; Sangwan, V. K.; Liu, X.; Lauhon, L. J.; Marks, T. J.; Hersam, M. C. Effective Passivation of Exfoliated Black Phosphorus Transistors against Ambient Degradation. *Nano Lett.* **2014,** *14*, 6964-6970.

19. Xu, J.; Chen, L.; Dai, Y.-W.; Cao, Q.; Sun, Q.-Q.; Ding, S.-J.; Zhu, H.; Zhang, D. W. A Two-Dimensional Semiconductor Transistor with Boosted Gate Control and Sensing Ability. *Sci. Adv.* **2017,** *3*, e1602246.

20. Shi, J.; Liang, W.-Y.; Raja, S. S.; Sang, Y.; Zhang, X.-Q.; Chen, C.-A.; Wang, Y.; Yang, X.; Lee, Y.-H.; Ahn, H.; Gwo, S. Plasmonic Enhancement and Manipulation of Optical Nonlinearity in Monolayer Tungsten Disulfide. *Laser Photonics Rev.* **2018,** *12*, 1800188.

21. Chen, H.; Corboliou, V.; Solntsev, A. S.; Choi, D.-Y.; Vincenti, M. A.; de Ceglia, D.; de Angelis, C.; Lu, Y.; Neshev, D. N. Enhanced Second-Harmonic Generation from Two-Dimensional $MoSe_2$ on a Silicon Waveguide. *Light Sci. Appl.* **2017,** *6*, e17060.

22. Wang, G.; Marie, X.; Gerber, I.; Amand, T.; Lagarde, D.; Bouet, L.; Vidal, M.; Balocchi, A.; Urbaszek, B. Giant Enhancement of the Optical Second-Harmonic Emission of WSe_2 Monolayers by Laser Excitation at Exciton Resonances. *Phys. Rev. Lett.* **2015,** *114*, 097403.

23. Seyler, K. L.; Schaibley, J. R.; Gong, P.; Rivera, P.; Jones, A. M.; Wu, S.; Yan, J.; Mandrus, D. G.; Yao, W.; Xu, X. Electrical Control of Second-Harmonic Generation in a WSe_2 Monolayer Transistor. *Nat. Nanotechnol.* **2015,** *10*, 407-411.

24. Li, D.; Huang, X.; Xiao, Z.; Chen, H.; Zhang, L.; Song, J.; Shao, D.-F.; Tsymbal, E. Y.; Lu, Y.; Hong, X. Evidence for Polar Symmetry Coupling at MoS_2/Ferroelectric Heterointerfaces. *arXiv preprint arXiv:1903.01664* **2019**.

25. Trolle, M. L.; Tsao, Y.-C.; Pedersen, K.; Pedersen, T. G. Observation of Excitonic Resonances in the Second Harmonic Spectrum of MoS_2. *Phys. Rev. B* **2015,** *92*, 161409.

26. Chen, J.; Wang, K.; Long, H.; Han, X.; Hu, H.; Liu, W.; Wang, B.; Lu, P. Tungsten Disulfide–Gold Nanohole Hybrid Metasurfaces for Nonlinear Metalenses in the Visible Region. *Nano Lett.* **2018,** *18*, 1344-1350.

27. Wang, Z.; Dong, Z.; Zhu, H.; Jin, L.; Chiu, M.-H.; Li, L.-J.; Xu, Q.-H.; Eda, G.; Maier, S. A.; Wee, A. T. Selectively Plasmon-Enhanced Second-Harmonic Generation from Monolayer Tungsten Diselenide on Flexible Substrates. *ACS Nano* **2018,** *12*, 1859-1867.

28. Chen, J.-h.; Tan, J.; Wu, G.-x.; Zhang, X.-j.; Xu, F.; Lu, Y.-q. Tunable and Enhanced Light Emission in Hybrid Ws2-Optical-Fiber-Nanowire Structures. *Light Sci. Appl.* **2019,** *8*, 8.

29. Fryett, T. K.; Seyler, K. L.; Zheng, J.; Liu, C.-H.; Xu, X.; Majumdar, A. Silicon Photonic Crystal Cavity Enhanced Second-Harmonic Generation from Monolayer WSe_2. *2D Mater.* **2016,** *4*, 015031.

30. Claudon, J.; Bleuse, J.; Malik, N. S.; Bazin, M.; Jaffrennou, P.; Gregersen, N.; Sauvan, C.; Lalanne, P.; Gérard, J.-M. A Highly Efficient Single-Photon Source Based on a Quantum Dot in a Photonic Nanowire. *Nat. Photonics* **2010,** *4*, 174.

31. Johlin, E.; Solari, J.; Mann, S. A.; Wang, J.; Shimizu, T. S.; Garnett, E. C. Super-Resolution Imaging of Light–Matter Interactions near Single Semiconductor Nanowires. *Nat. Commun.* **2016,** *7*, 13950.

32. Johlin, E.; Mann, S. A.; Kasture, S.; Koenderink, A. F.; Garnett, E. C. Broadband Highly Directive 3D Nanophotonic Lenses. *Nat. Commun.* **2018,** *9*, 4742.

33. Säynätjoki, A.; Karvonen, L.; Rostami, H.; Autere, A.; Mehravar, S.; Lombardo, A.; Norwood, R. A.; Hasan, T.; Peyghambarian, N.; Lipsanen, H. Ultra-Strong Nonlinear Optical Processes and Trigonal Warping in MoS_2 Layers. *Nat. Commun.* **2017,** *8*, 893.

34. Wang, Z.; Dong, Z.; Gu, Y.; Chang, Y.-H.; Zhang, L.; Li, L.-J.; Zhao, W.; Eda, G.; Zhang, W.; Grinblat, G. Giant Photoluminescence Enhancement in Tungsten-Diselenide–Gold Plasmonic Hybrid Structures. *Nat. Commun.* **2016,** *7*, 11283.

35. Kumar, S.; Verma, N. K.; Singla, M. L. Study on Reflectivity and Photostability of Al-Doped TiO_2 Nanoparticles and Their Reflectors. *J. Mater. Res.* **2013,** *28*, 521-528.

36. Hendry, E.; Hale, P. J.; Moger, J.; Savchenko, A.; Mikhailov, S. A. Coherent Nonlinear Optical Response of Graphene. *Phys. Rev. Lett.* **2010,** *105*, 097401.

37. Li, X.-L.; Han, W.-P.; Wu, J.-B.; Qiao, X.-F.; Zhang, J.; Tan, P.-H. Layer-Number Dependent Optical Properties of 2D Materials and Their Application for Thickness Determination. *Adv. Fun. Mater.* **2017,** *27*, 1604468.

38. Pu, Y.; Grange, R.; Hsieh, C.-L.; Psaltis, D. Nonlinear Optical Properties of Core-Shell Nanocavities for Enhanced Second-Harmonic Generation. *Phys. Rev. Lett.* **2010,** *104*, 207402.

39. Yu, Y.; Yu, Y.; Xu, C.; Cai, Y. Q.; Su, L.; Zhang, Y.; Zhang, Y. W.; Gundogdu, K.; Cao, L. Engineering Substrate Interactions for High Luminescence Efficiency of Transition-Metal Dichalcogenide Monolayers. *Adv. Fun. Mater.* **2016,** *26*, 4733-4739.

40. Zeng, J.; Li, J.; Li, H.; Dai, Q.; Tie, S.; Lan, S. Effects of Substrates on the Nonlinear Optical Responses of Two-Dimensional Materials. *Opt. Express* **2015,** *23*, 31817-31827.

41. Ugeda, M. M.; Bradley, A. J.; Shi, S.-F.; Felipe, H.; Zhang, Y.; Qiu, D. Y.; Ruan, W.; Mo, S.-K.; Hussain, Z.; Shen, Z.-X. Giant Bandgap Renormalization and Excitonic Effects in a Monolayer Transition Metal Dichalcogenide Semiconductor. *Nat. Mater.* **2014,** *13*, 1091.

42. Kumar, N.; Najmaei, S.; Cui, Q.; Ceballos, F.; Ajayan, P. M.; Lou, J.; Zhao, H. Second Harmonic Microscopy of Monolayer MoS_2. *Phys. Rev. B* **2013,** *87*, 161403.

43. Liang, J.; Zhang, J.; Li, Z.; Hong, H.; Wang, J.; Zhang, Z.; Zhou, X.; Qiao, R.; Xu, J.; Gao, P. Monitoring Local Strain Vector in Atomic-Layered Mose2 by Second-Harmonic Generation. *Nano Lett.* **2017,** *17*, 7539-7543.

44. Zhang, X.-Q.; Lin, C.-H.; Tseng, Y.-W.; Huang, K.-H.; Lee, Y.-H. Synthesis of Lateral Heterostructures of Semiconducting Atomic Layers. *Nano Lett.* **2014,** *15*, 410-415.

45. Hsu, W.-T.; Zhao, Z.-A.; Li, L.-J.; Chen, C.-H.; Chiu, M.-H.; Chang, P.-S.; Chou, Y.-C.; Chang, W.-H. Second Harmonic Generation from Artificially Stacked Transition Metal Dichalcogenide Twisted Bilayers. *ACS Nano* **2014,** *8*, 2951-2958.

46. Mennel, L.; Furchi, M. M.; Wachter, S.; Paur, M.; Polyushkin, D. K.; Mueller, T. Optical Imaging of Strain in Two-Dimensional Crystals. *Nat. Commun.* **2018,** *9*, 516.

47. Peng, Q.; De, S. Outstanding Mechanical Properties of Monolayer MoS_2 and Its Application in Elastic Energy Storage. *Phys. Chem. Chem. Phys.* **2013,** *15*, 19427-19437.

48. Cooper, R. C.; Lee, C.; Marianetti, C. A.; Wei, X.; Hone, J.; Kysar, J. W. Nonlinear Elastic Behavior of Two-Dimensional Molybdenum Disulfide. *Phys. Rev. B* **2013,** *87*, 035423.

49. Naik, M. H.; Jain, M. Ultraflatbands and Shear Solitons in Moir\'E Patterns of Twisted Bilayer Transition Metal Dichalcogenides. *Phys. Rev. Lett.* **2018,** *121*, 266401.

50. Cao, Y.; Fatemi, V.; Demir, A.; Fang, S.; Tomarken, S. L.; Luo, J. Y.; Sanchez-Yamagishi, J. D.; Watanabe, K.; Taniguchi, T.; Kaxiras, E.; Ashoori, R. C.; Jarillo-Herrero, P. Correlated

Insulator Behaviour at Half-Filling in Magic-Angle Graphene Superlattices. *Nature* **2018,** *556*, 80.

51. Bistritzer, R.; MacDonald, A. H. Moiré Bands in Twisted Double-Layer Graphene. *P. Natl. Acad. Sci.* **2011,** *108*, 12233-12237.

Table of Contents Graphic